applied sciences

MDPI

Article

THz Radiation Measurement with HTSC Josephson Junction Detector Matched to Planar Antenna

Eldad Holdengreber [1,*], Aviv Glezer Moshe [2,3], Shmuel E. Schacham [4], Moshe Mizrahi [4], Dhasarathan Vigneswaran [5] and Eliyahu Färber [2,4]

1 Department of Mechanical Engineering & Mechatronics, Ariel University, Ariel 40700, Israel
2 Department of Physics, Ariel University, Ariel 40700, Israel; avivmoshe@mail.tau.ac.il (A.G.M.); e.farber@ariel.ac.il (E.F.)
3 School of Physics and Astronomy, Tel Aviv University, Tel Aviv 6997801, Israel
4 Department of Electrical & Electronic Engineering, Ariel University, Ariel 40700, Israel; schacham@ariel.ac.il (S.E.S.); mosheme@ariel.ac.il (M.M.)
5 Department of ECE, Sri Krishna College of Technology, Coimbatore 641042, India; dhasa.viki@gmail.com
* Correspondence: eldadh@ariel.ac.il

Received: 12 August 2020; Accepted: 15 September 2020; Published: 17 September 2020

Featured Application: Experimental results prove that major improvement of THz radiation detection can be obtained by the optimal design of planar antenna with HTSC Josephson junction. Matching between the low impedance of the junction and the high impedance of the antenna is attainable, resulting in a high efficiency detection system, while enjoying the drastic reduction of system complexity of a THz radiation detection by a Josephson junction.

Abstract: Superconducting Josephson junctions have major advantages as detectors of millimeter wave radiation. Frequency of the radiation can be easily derived from the Shapiro steps of the current-voltage characteristics. However, system performance is highly sensitive to impedance mismatch between the antenna and the junction; therefore, optimization is essential. We analyzed and implemented an improved antenna structure, in which the junction is displaced from the antenna center and placed between the ends of two matching strips. Based on theoretical analysis and advanced electromagnetic simulations, we optimized strip dimensions, which affect both the detection magnitude and the frequency of the reflection coefficient dip. Accordingly, two Au bow-tie antennas with different matching strip widths were fabricated. Superconducting Yttrium Barium Copper Oxide (YBCO) thin films were deposited exactly at the bicrystal substrate misorientation points, forming Josephson junctions at the ends of two matching strips. We found a very high correlation between the simulations and the response to Radio Frequency (RF) radiation in the range of 145–165 GHz. Experimental results agree extremely well with the design, showing best performance of both antennas around the frequency for which impedance matching was derived.

Keywords: THz sources and detectors; antennas; Josephson junctions; millimeter wave radiation

1. Introduction

Due to the ever-increasing requirements of communication systems, there is an increasing demand for systems in the millimeter wave range [1]. This range is also applicable to medicine, biology, astronomy, defense and materials technology [2,3]. However, realization of high frequency communication systems in the THz range becomes extremely complex. Implementation of sources and detectors in this range is very complicated [4,5]. Moreover, conventional communication techniques are incompatible with these high frequencies. On the other hand, photon energies are too low for adopting optical approaches. As a result, detection of millimeter wave radiation necessitates the development of new technologies of transmission and reception.

Junctions in superconducting materials can be implemented by depositing a superconducting layer over a discontinuity in the material structure, such as in step-edge [6]. These junctions are known as Josephson junctions. A unique feature of superconducting junctions, which has important applications for detection of RF radiation, is the Shapiro steps. These current steps are the result of the modulation by RF radiation of the current flowing through the junction. They are observed when measuring the I-V (Current-Voltage) characteristics of the Josephson junction.

The measurements of the Shapiro steps and the RF analysis are carried-out using simple Direct Current (DC) equipment [7]. As a result, the complexity and cost of detection systems for high frequency radiation are significantly reduced in comparison with common THz detection systems [2]. Thus, superconducting Josephson junctions are well suited to serve as detectors of millimeter wave radiation [7]. They provide a technique for measurement of intensity and frequency of high frequency signals, without resorting to complex electronics, such as high frequency spectrum analyzers [8,9].

A major breakthrough in application of superconductivity was achieved with the discovery of High Temperature Superconductors (HTSC) materials, in which superconductivity can be obtained at higher temperatures, including liquid nitrogen temperatures. The first and most applicable family of HTSC materials are the YBCO [10]. The realization of high frequency Josephson junction detectors in HTSC, reduces drastically the intricacy of the detector systems. Inexpensive cryogenic systems, cooling down to liquid nitrogen temperature range, suffice for turning the material into a superconductor [11,12].

A serious drawback of detection systems based on superconducting junctions is their low efficiency [13,14]. This results in lower system sensitivity, higher electrical noise-equivalent-power (NEP), and lower coupled power voltage responsivity, $\eta(V)$ [8,9]. In addition, the performance of millimeter wave detector systems depends strongly on the exact structure and geometry of the antenna [3,4]. The antenna must have a wide aperture and a high gain [15].

Another problem with detection systems based on HTSC Josephson junction is impedance mismatch between the junction and the antenna, due to the very low impedance of the junction (few Ohms) [8,16,17]. The impedance mismatch can be detrimental to the performance of the detector [18]. To reduce losses, the impedance of these two elements must be matched. Optimization of the interface between the detector and the antenna is essential. Moreover, detectors implemented in HTSC are more sensitive to the tolerances of production than those based on low temperature superconductors, due to the shorter coherence length at HTSC junctions [19].

In this paper, we present the analysis and implementation of a THz antenna system, combining a superconducting Josephson junction with a bow-tie antenna. Bow-tie antennas are the preferred architecture for the high performance of THz transmission and detection, with broadband, efficient radiation characteristics [20]. The size and the shape of these antennas make them ideal for interfacing with communication modules and detectors [21,22]. Indeed, previous studies and measurements have shown that antennas of this type can be very suitable for THz detection systems [23,24].

To obtain impedance matching we introduce an improved structure, in which the junction detector is not placed in the center of the antenna [25]. Instead, the junction is placed at the end of two matching strips remote from the center. The basic concept and simulations, for several configurations, have been presented in previous works [26–30]. In this work, we present the implementation and characterization of THz detectors based on this structure.

The investigation starts with a theoretical analysis, exploring the influence of the junction parameters on the input impedance of the antenna, as described in Section 2.1. Using extensive simulations based on this analysis, we were able to optimize the system design, including the antenna structure, the matching strip dimensions, and the junction configuration, as detailed in Section 2.2. The various parameters of Josephson junctions, including the junction geometry, impedance, and substrate effects, were taken into account in the simulations [31].

In order to examine the effects of impedance matching on the performance of the detection system, we implemented two bow-tie antennas with different matching strip width. The configuration of the two systems was based on the results of our simulations. The HTSC junctions were implemented by growing a thin film of $YBa_2Cu_3O_7$ on the substrate. Layers of YBCO thin films and Au were deposited over the (100)MgO bicrystal substrate, by Theva GmbH, Germany [32]. In the space between the two antenna poles, only the Au layer was etched, exposing a thin layer of YBCO. Thus, the YBCO Josephson junction was located exactly at the bicrystal misorientation point. The final structure of the planar antenna and the detector was obtained by etching of these layers, performed by STAR Cryoelectronics, USA [33]. In Section 3, we present experimental results, demonstrating the high performance of the fabricated antennas.

2. Materials and Methods

2.1. Josephson Junction as an RF Element in Cascade Reception Chain

In order to develop the model for the simulations of a superconducting antenna system, we investigated the circuit representation of the detector. The current flowing through the junction I_S is the superposition between the DC current supplied to the junction, and the current generated by the RF radiation. Neglecting noise, I_S can be expressed in terms of Bessel functions of the first kind J_m [9]:

$$I_S = I_C \sum\nolimits_{m=-\infty}^{\infty} (-1)^m J_m\left(\frac{2eV_{RF}}{\hbar\omega_{RF}}\right) \sin\left(\left(\frac{2eV_{DC}}{\hbar} - m\omega_{RF}\right)t + \varphi_0\right) \tag{1}$$

The RF radiation generates steps in the I-V characteristics, known as the Shapiro steps. The height of the steps is proportional to the voltage amplitude of the radiation V_{RF} [34,35]. It reflects the detection efficiency, as affected by the integration between the antenna and the Josephson junction detection element. The voltage separation V_m between the steps gives an accurate measure of the radiation frequency ω_{RF}, obtained from $V_m = m\frac{\hbar}{2e}\omega_{RF}$.

The current flowing through the junction is a superposition of three components: the normal current, I_R, the charging current, I_{ch}, and the Josephson supercurrent, I_{JJ}. Since the current supplied to the junction is larger than the critical current I_c, the superconductor is not in its classic superconducting state, i.e., the junction has a parallel normal component that behaves as a resistor R_n.

We analyze the interrelations between the input impedance, Z_{in}, the antenna impedance, Z_A, and the Josephson junction equivalent impedance, Z_{JJ}. This relation is derived through a cascade chain connection of two "2 port network" models, using an equivalent ABCD matrix [27]. Figure 1 shows the layout of the networks. Network$^{\alpha}$ represents the junction network, and network$^{\beta}$ represents the antenna network.

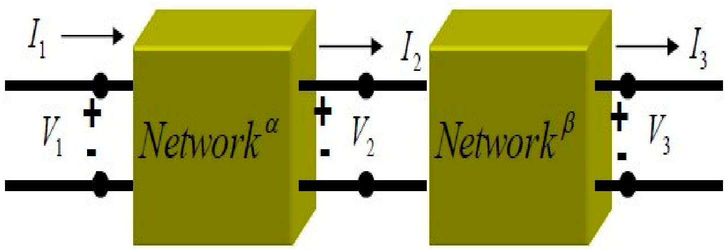

Figure 1. Cascade, chain connection, of two "2 port network".

One can express the integration between these networks through the voltage/current matrix relationship.

$$[\alpha] = \begin{bmatrix} 1 & 0 \\ \frac{1}{Z_{JJ}} & 1 \end{bmatrix} = \begin{bmatrix} 1 & 0 \\ \frac{1}{R_n} + j\omega C_J & 1 \end{bmatrix} \tag{2}$$

$$[\beta] = Z_A \tag{3}$$

Equations (2) and (3) describe the network matrices, the junction ABCD matrix $[\alpha]$, and the antenna impedance matrix $[\beta]$. From these equations, we derive an expression for the input impedance,

$$Z_{in} = \frac{V_1}{I_1} = \frac{AV_2 + BI_2}{CV_2 + DI_2} = \frac{Z_A}{\frac{Z_A}{R_n} + 1 + j\omega C_J Z_A} \tag{4}$$

Z_{JJ}, can be written in terms of electromagnetic wave propagation as [8]:

$$Z_{JJ} = \frac{c}{\bar{c}}\left(\frac{l}{w\varepsilon_{rs}}\right)Z_0 \tag{5}$$

where Z_0 = 377 Ω is the free space impedance. w and l are the width and length of the junction, ε_{rs} is the relative dielectric constant of the junction, c is the speed of light in free space. The speed of light in a medium $\bar{c}$, is given by: $\bar{c} = c\sqrt{\frac{l}{l'\varepsilon_{rs}}}$, where the effective length of the junction, is given by $l' = l + \lambda_{L1} + \lambda_{L2}$. The London penetration depth for both sides of the junction is given by $\lambda_L = \sqrt{\frac{m_e}{\mu_0 n_s e^2}}$, where m_e is the electron mass, μ_0 is the permeability of free space, n_s is the density of superconducting charge carriers, and e is the electron charge. Using Equations (4) and (5) we can express the dependence of Z_{in} on junction dimensions as:

$$Z_{in} = \frac{Z_A}{\frac{\bar{c}}{c}\left(\frac{w\varepsilon_r}{Z_0 l}\right)Z_A + 1} \tag{6}$$

The optimal input impedance for impedance matching is obtained by selecting the proper dimensions of the antenna and matching strips, thus setting the value of Z_A in Equation (6).

2.2. Antenna Optimization

The bow-tie antenna is composed of a two-part bow-tie shape, designed to reduce the reflection coefficient. It is characterized by broad-band impedance [15,20]. The performance of the detection systems is analyzed by electromagnetic simulations, carried out using High-Frequency Structure Simulator (HFSS) software by ANSYS. We begin with the analysis of the conventional design, in which the Josephson junction is placed in the gap between the two poles of the antenna [12,25]. Optimal results were obtained for a pole width of 115.5 µm and a length of 144.3 µm, with a separation between the two antenna poles, a gap width, of a 4.2 µm. The efficiency of such systems deteriorates rapidly at very high frequencies, due to impedance mismatch between the antenna and the junction. Figure 2 shows the simulation results of the reflection coefficient S_{11} as a function of frequency. The simulation renders a bandwidth of about 4 GHz, at 3.57:1 voltage standing wave ratio (VSWR), showing a power ratio of up to 0.874 for the power supplied to the antenna, i.e., an efficiency of 87.4% not including ohmic losses. The reflectivity obtained is around −11 dB at the central frequency of 148 GHz.

We propose a new structure in which the junction is placed between the ends of two matching strips, as outlined in Figure 3. This structure is intended to enable, with proper optimization of the strip dimensions, high impedance matching at high frequencies between the antenna input impedance Z_{in} and the junction impedance Z_{JJ}.

Figure 4 shows the structure of a two-pole antenna, as designed and built in the simulation software. The poles consist of a 250 nm thick Au layer on top of a 330 nm thick YBCO layer and 0.5 mm thick MgO substrate. Other parameters included in the simulations are the dielectric constant of the MgO substrate, ε_r = 9.8, and the loss tangent, tanδ, approximately 10^{-4} at 77 K [36,37]. The antenna dimensions were modified in order to obtain a high gain and a low reflection coefficient. Optimal results were obtained for a pole width of 75.5 µm and a length of 74 µm. The separation between the two antenna poles, the gap width, is 4.2 µm.

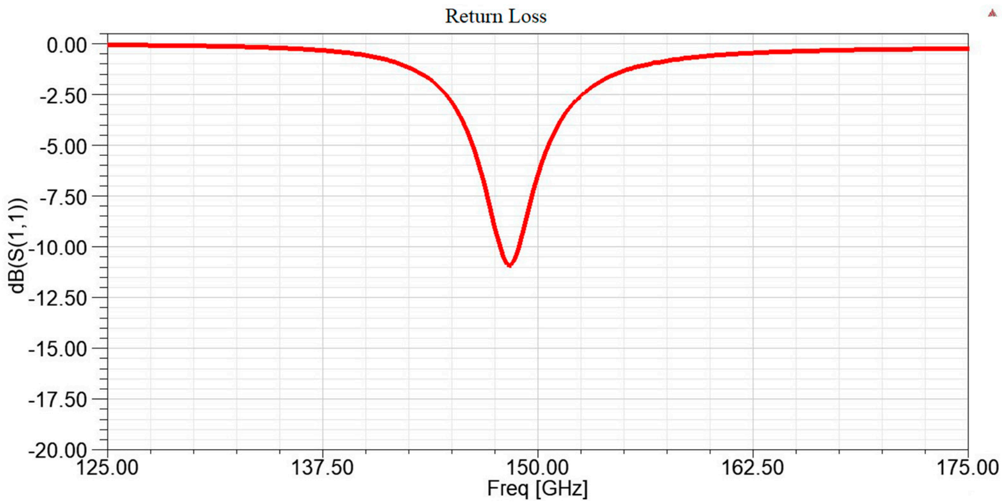

Figure 2. Reflection coefficient, S_{11}, for conventional bow-tie antenna, as function of frequency.

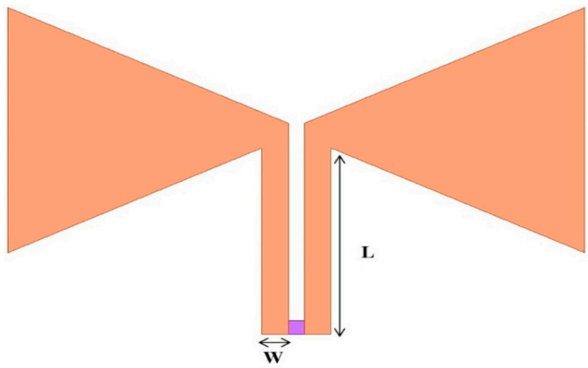

Figure 3. Geometry of bow-tie antenna. L is the length of the matching impedance strips and W its width. The junction is placed between the bottom ends of the strips (purple rectangle).

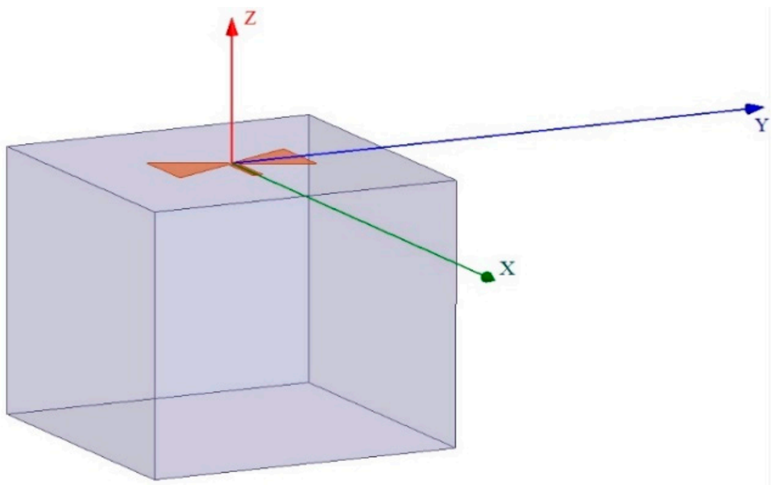

Figure 4. Structure of bow-tie antenna in HFSS software.

Figure 5 shows the results of simulations for the reflection coefficient S_{11}, as a function of frequency, with matching strips 4.6 µm wide each, for various values of length (L in Figure 3). In order to evaluate the junction equivalent impedance Z_{JJ}, we used typical parameters for bicrystal Josephson junctions [31,38]. The light velocity ratio $\bar{c}/c$ is estimated to be around 0.03 [8,31] with a relative dielectric constant, ε_{rs}, of 5 for the YBCO [38]. The junction width w was set to 4.2 µm. Inserting these values into Equation (3), one obtains $Z_{JJ} = \frac{1}{0.03}\left(\frac{l}{4.2 \cdot 10^{-6} \cdot 5}\right) \cdot 377\ \Omega$. Thus, for $l \cong 3.5$ nm, $Z_{JJ} \cong 2\ \Omega$. The lowest reflection coefficient was obtained for an antenna with $L = 108$ µm. The simulation renders a bandwidth of ~4 GHz, at 2.615:1 VSWR, with an efficiency of up to 99.75%, not including ohmic losses. For this structure, the calculated reflection coefficient is −26 dB at the central frequency of 155 GHz.

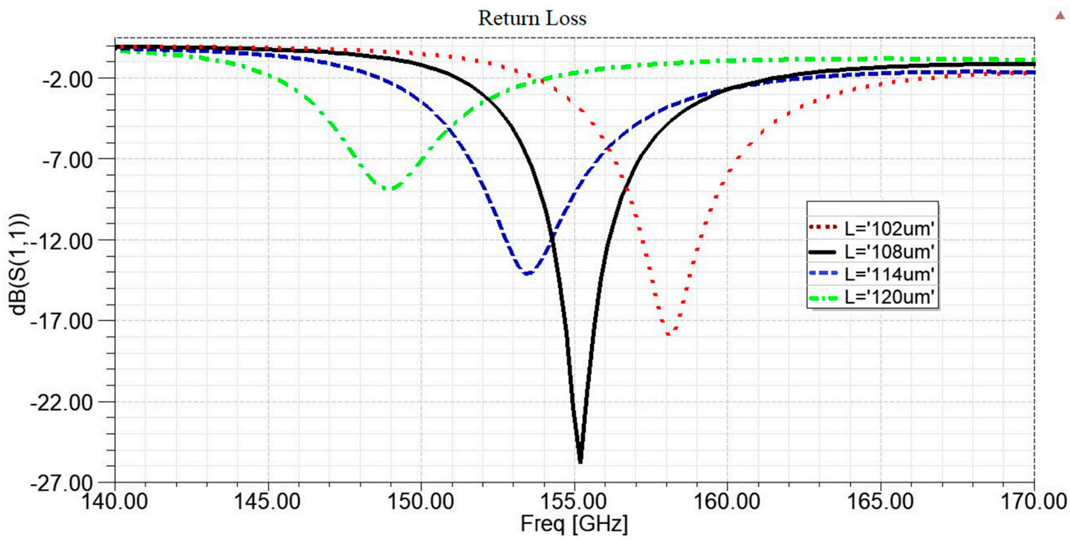

Figure 5. Antenna reflection coefficient S_{11} vs. frequency for various matching strips lengths. W = 4.6 µm.

Simulation results presented in Figure 5 were performed assuming a known value of the junction impedance: Z_{JJ}. However, it should be pointed out that according to Equation (6), this impedance is most sensitive to the exact value of the length of the junction l.

Figure 6 shows the reflection coefficient as a function of frequency, for several values of Z_{JJ}. Simulation results show that the system performance deteriorates rapidly for Z_{JJ} values different from those required for optimal impedance matching conditions. The system efficiency drops from 99.75% for $Z_{JJ} \cong 2\ \Omega$ to 95% for $Z_{JJ} \cong 1\ \Omega$ and down to 80% for $Z_{JJ} \cong 0.6\ \Omega$, excluding ohmic losses. The mismatch is also reflected in a shift of the central frequency.

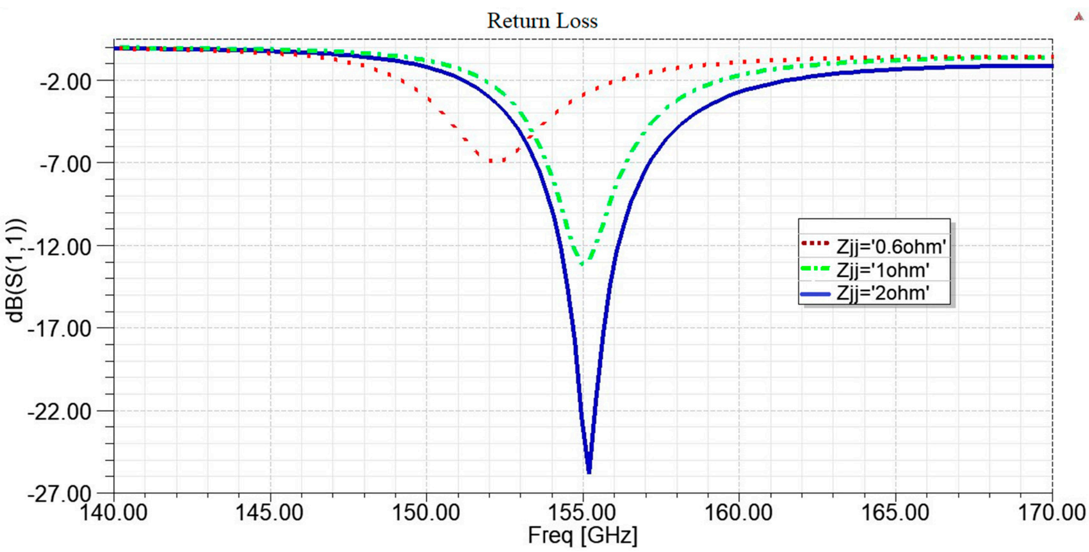

Figure 6. Reflection coefficient S_{11} vs. frequency for various values of Josephson junction characteristic impedance Z_{JJ} for bow-tie antenna.

Figure 7 shows the real (continuous blue line) and the imaginary (red dots) parts of the antenna input impedance Z_{in} for a structure with matching strips 4.6 μm wide and 108 μm long, as a function of frequency. Clearly, Z_{in} is highly correlated to the junction impedance Z_{JJ} around 155 GHz, reaching high impedance matching at this frequency.

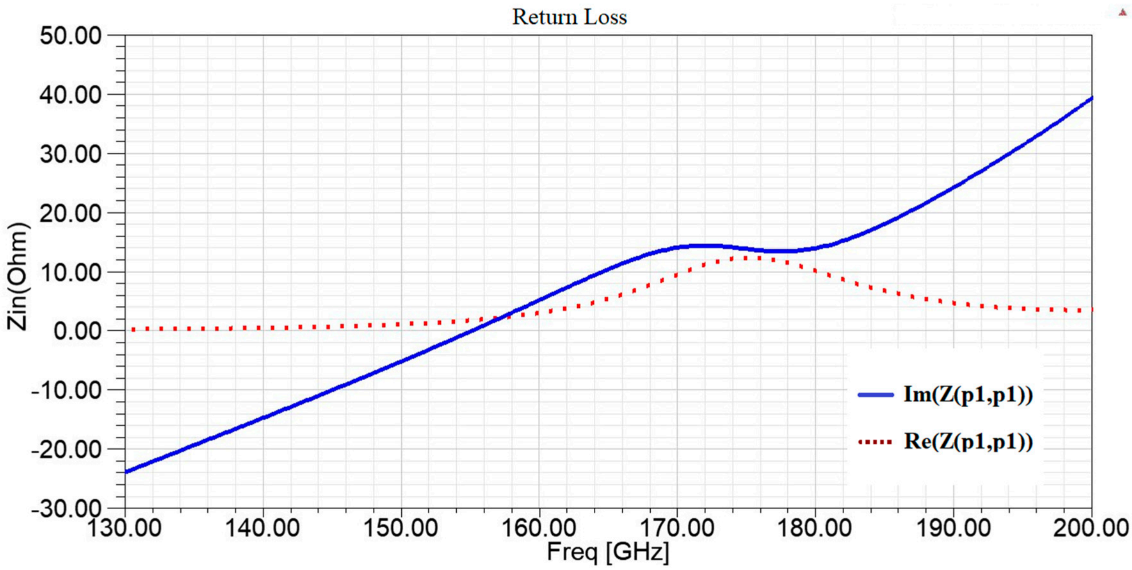

Figure 7. Antenna input impedance Z_{in} vs. frequency for L = 108 μm, W = 4.6 μm.

Figure 8 shows the radiation pattern and gain power, 2-D far-field pattern, at the central frequency of 155 GHz. The antenna gain is around 2.8 dBi in the $-Z$ axis, better than the gain of 2.5 dBi along the opposite direction.

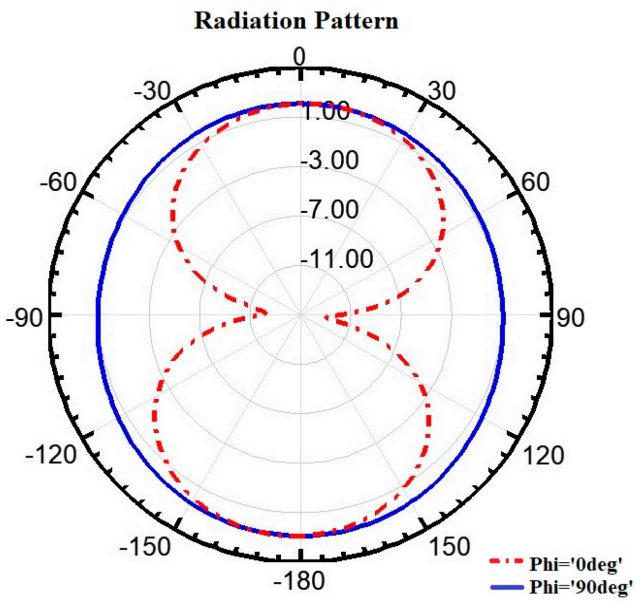

Figure 8. Simulation of 2-D radiation pattern at 155 GHz, phi is the angle perpendicular to the x axis (Figure 4).

Figure 9 shows the results of simulations for the reflection coefficient S_{11}, as a function of frequency, for antennas with a strips length of 108 μm, for various values of matching strips width W. Here, the lowest reflection coefficient was obtained for an antenna with a strip width of 4.6 μm. This simulation renders a bandwidth of ~4 GHz, at 2.615:1 VSWR, with an efficiency of up to 99.75%, not including ohmic losses. The reflection coefficient obtained is −26 dB at a central frequency of 155 GHz. A very strong dependence of reflection coefficient on the width of the matching strips is observed. This correlation is more pronounced in determining the central frequency of the detection system, which emphasizes the need for a great precision in the production process of such a detection system.

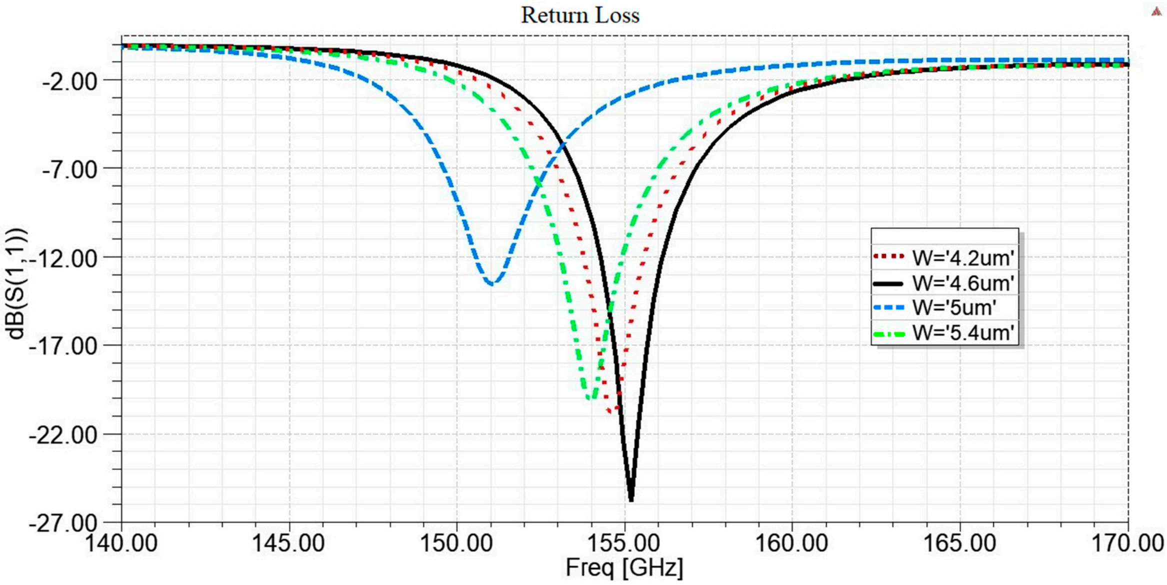

Figure 9. Reflection coefficient S_{11} vs. frequency for various matching strips widths without a lens. L = 108 µm.

To improve the directivity of the antenna, a silicon (Si) hemispherical lens, 1 mm in diameter, was added in the simulations, as demonstrated in Figure 10 [39,40]. The lens was placed on the backside −Z direction of the MgO substrate, to prevent potential damage to the junction located in the center of the antenna.

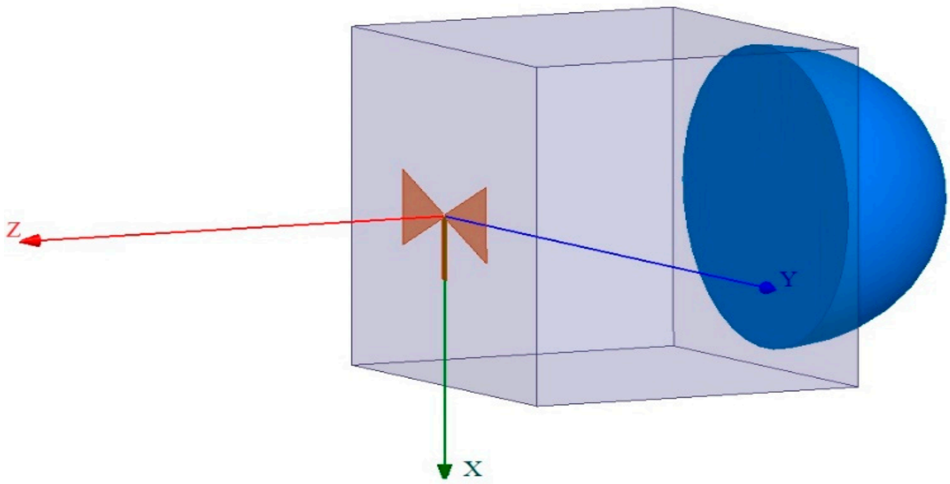

Figure 10. Structure of antenna with a Si lens.

Figure 11 shows the simulation results for the reflection coefficient, obtained for the antenna with a Si lens, with matching strips length L of 108 µm, for various values of strips width W. As in the previous case, the lowest reflection was obtained for an antenna with a width of 4.6 µm. The simulation renders a bandwidth of ~3.4 GHz, at 2.615:1 VSWR, with an efficiency of up to 99.2%, not including ohmic losses. The reflectivity obtained is −21 dB at the central frequency of 148.2 GHz.

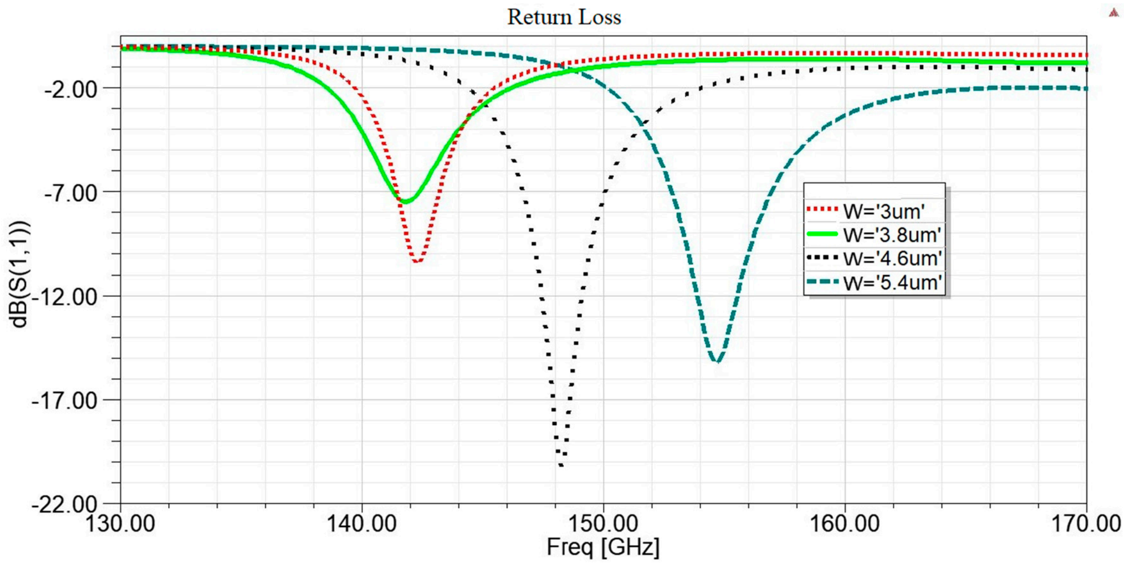

Figure 11. Reflection coefficient S_{11} vs. frequency for various matching strips widths of antennas with a Si lens. L = 108 μm.

Figure 12 shows the radiation curve and gain power, 2-D far-field pattern, at the central frequency of 148.2 GHz. The radiation pattern indicates the lower gain power along the Z axis, i.e., the antenna performance is inferior in that direction, as compared with the gain of 6.2 dBi along the $-Z$ axis. In order to obtain high performance, the detector should be positioned pointing in the $-Z$ direction relative to the radiation source.

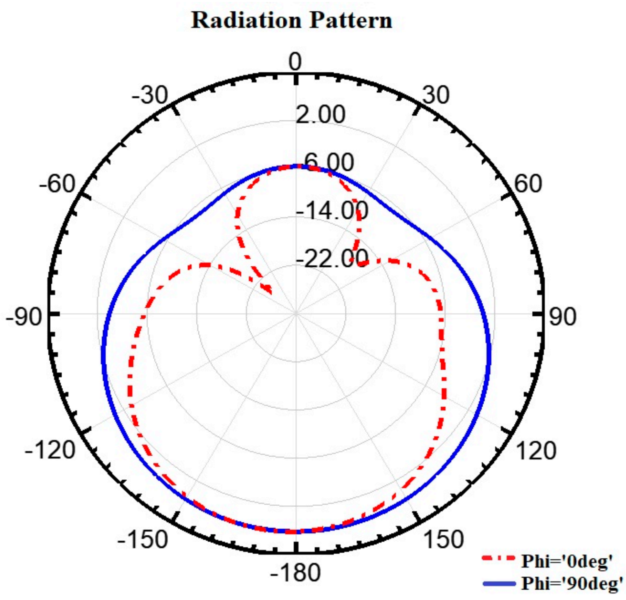

Figure 12. 2-D radiation pattern simulation at 148.2 GHz, phi is the angle perpendicular to the x axis (Figure 10).

3. Experimental Results

Two bow-tie antennas, along with matching strips, were implemented. The widths of the strips, 4.6 μm and 5.4 μm, were set according to the best results obtained in our theoretical analysis. We tested the performance of the antennas with and without a Si lens. The frequency response of the antennas was measured using a Backward Wave Oscillator (BWO) THz source. The antennas were placed inside a quasi-optic cryogenic cooling system, thereby the Josephson junctions operated at 60 K, below their critical temperature. We measured the I-V characteristics of the antenna system by radiating it with RF signals in the range of 145–165 GHz.

3.1. Experimental Setup

The measurement setup includes a BWO THz source, quasi-optical lenses to focus the radiated RF signal on the detector, a cryogenic cooling system with high-density polyethylene windows, and a Tektronix company Keithley Nano-voltmeter and current source (Figure 13). The Cryo Industries cryogenic cooling system enables testing the performance of the device at low temperatures, down to ~2 K. An important advantage of this cooling system is that the devices inside the chamber do not touch directly the liquid helium used for cooling, thus preventing contamination of the device. The BWO source is a miniature electrovacuum device placed in a metal packaging. When the BWO source is in a magnetic field and supplied with high voltage (up to 6.5 kV), it emits monochromatic electromagnetic radiation, with a power of up to ~10 mW, depending on the supplied voltage and magnetic field frequency and strength [41]. A photo and a discerption of the measurement setup is presented in the Appendix A.

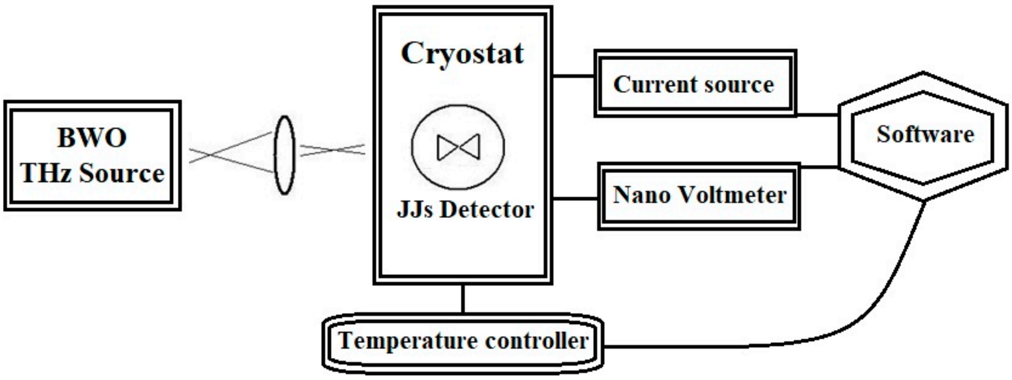

Figure 13. Measurement setup block diagram.

3.2. Measurement Results

We evaluated the sensitivity of the Josephson detector according to its NEP, based on the relation $\frac{NEP}{\sqrt{\Delta V}} = \sqrt{6}\left(\frac{\hbar\omega_{RF}}{2eR_nI_c}\right)^2\sqrt{4k_BTR_n}$. R_n is the normal resistance, I_c is the critical current in the presence of the RF radiation, and ω_{RF} is the radiation frequency. The coupled power voltage responsivity $\eta(V)$ was derived from $\eta(V) = \frac{\Delta V}{P_{RF}}$ where P_{RF} is the amplitude of the RF power coupled into the junction. P_{RF} can be estimated from the amplitude of the RF current, $I_{RF} = \frac{\hbar\omega_{RF}\sqrt{I_{c0}\Delta I}}{eR_nI_c}$ [7–9]. I_{c0} is the unsuppressed critical current, without RF radiation. $\hbar$ is Planck constant divided by 2π, and e is the electron charge. $\Delta V = R_d(V)\Delta I$, where ΔI is the change in the junction current due to the RF signal. $R_d(V)$ is the dynamic resistance, $\Delta V/\Delta I$.

Figure 14 shows the measured I-V and dI/dV characteristics for the antenna with a 4.6 µm wide matching strip. The data was taken at 60 K without a Si lens. The unsuppressed critical current is $I_{c0} \approx 1$ mA and the normal resistance $R_n \approx 3.5\ \Omega$. The top curve shows the junction response to the RF signal at 155 GHz, showing a critical current $I_c \approx 0.75$ mA. The estimated electrical NEP for the detector is ~4×10^{-12} W·Hz$^{-1/2}$. The RF current, I_{RF}, is estimated to be ~0.1 mA, thus the voltage responsivity is $\eta(V) \approx 33$ kV·W^{-1}. The Shapiro step at 0.32 mV is due to the presence of an electromagnetic radiation at ~155 GHz. The dI/dV characteristics (bottom curve Figure 14) shows the RF response of the junction to signals at various frequencies. The measured narrow bandwidth high peak at 155 GHz, as well as the poor performance at other frequencies, are a clear indication of the high accuracy of our simulations. The high frequency selectivity of the detector system is demonstrated clearly by the set of peaks, shown in the bottom figure.

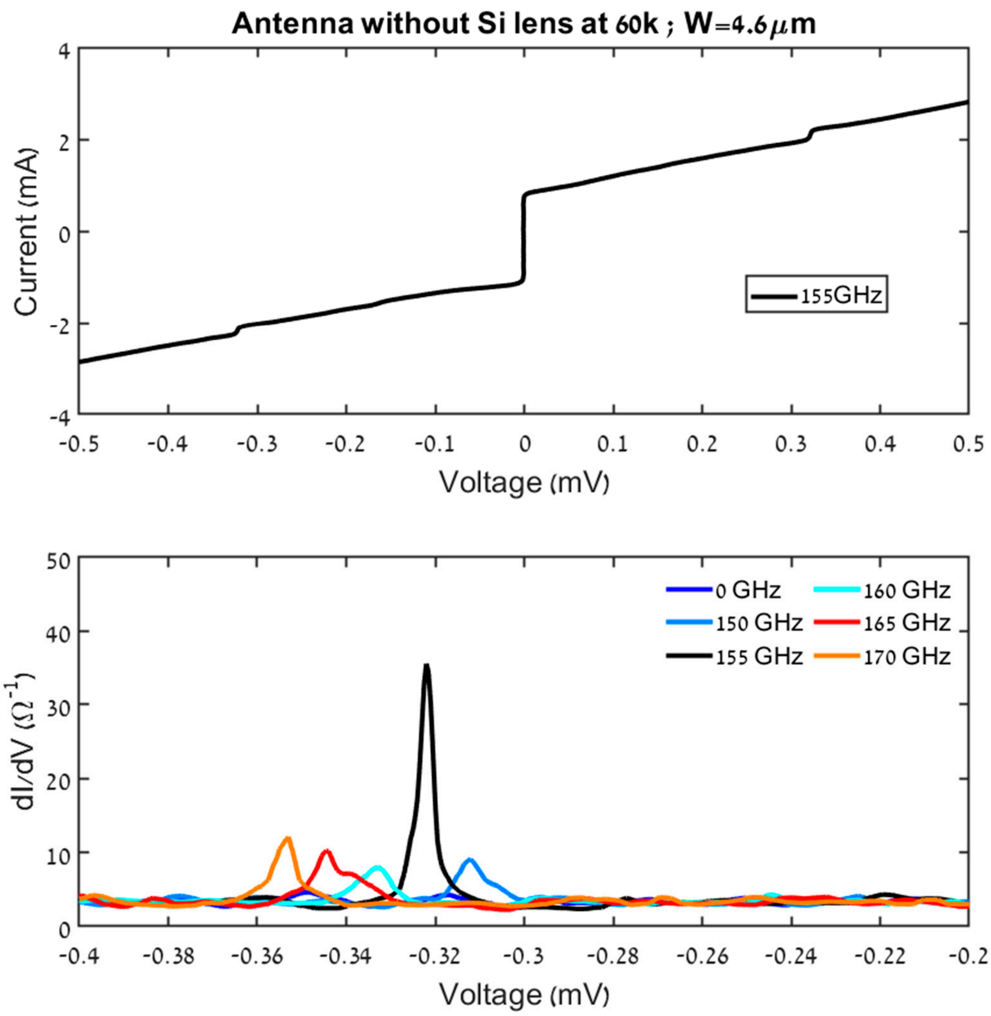

Figure 14. I-V (**top figure**) and dI/dV (**bottom figure**) characteristics measured at 60 K for antenna with a 4.6 μm wide matching strip, without a lens.

Figure 15 show the I-V and dI/dV characteristics of the same antenna, measured at 60 K, but with a Si lens. The top curve presents the junction response to an RF signal at 148.2 GHz, showing a critical current of $I_c \approx 0.4$ mA. The estimated NEP is ~1×10^{-13} W·Hz$^{-1/2}$. The RF current, I_{RF}, can be estimated as ~0.3 mA, thus the voltage responsivity is $\eta(V) \approx 55$ kV·W^{-1}. The Shapiro step at 0.31 mV is due to the presence of electromagnetic radiation at ~148 GHz. These results are clearly superior to typical NEP and $\eta(V)$ values reported for sensitive detection systems at 60 K, namely around 1×10^{-12} W·Hz$^{-1/2}$ and 10 kV·W^{-1}, respectively [13,25,42]. Once again, the high peak at 148 GHz in the dI/dV characteristics (bottom curve Figure 15) demonstrates the high agreement between simulation and experimental results. One can see that using Si lens the center frequency of the matched antenna has shifted, as predicted by the electromagnetic simulations.

Figure 16 shows the measured I-V and dI/dV characteristic of the second antenna implemented with matching strips width of 5.4 μm. The measurements were taken at 60 K, with a Si lens. The unsuppressed measured critical current is $I_{c0} \approx 1.93$ mA, a relatively high value for a bicrystal junction. The normal resistance is $R_n \approx 3.8\ \Omega$. This higher critical current reduces the sensitivity of the detector. The measured peak at 155 GHz agrees extremely well with the theoretical results shown in Figure 11, proving that the impedance matching between the antenna and the junction was not affected. The top curve shows the junction response to an RF signal at 155 GHz, demonstrating a critical current $I_c \approx 1.52$ mA. The estimated electrical NEP for the detector is ~1×10^{-12} W·Hz$^{-1/2}$. The RF current, I_{RF}, can be estimated to be ~0.1 mA, thus the voltage responsivity $\eta(V) \approx 40$ kV·W^{-1}. The Shapiro step at 0.32 mV indicates the presence of electromagnetic radiation at ~155 GHz.

The dI/dV characteristics (bottom curve Figure 16) show the junction RF response for signals at various frequency values. The high peak at 155 GHz demonstrates the high correlation between simulation and experimental results. It is clear that the performance of the antenna with 5.4 µm wide matching strips is inferior to the performances of the first antenna. This is most likely due to a combination of two reasons: the 4.6 µm width is the optimal design for minimal reflection coefficient, as seen in Figure 11, and the quality of the Josephson junction is not as high as the previous one. This results also in low quality data measured without a lens for this antenna.

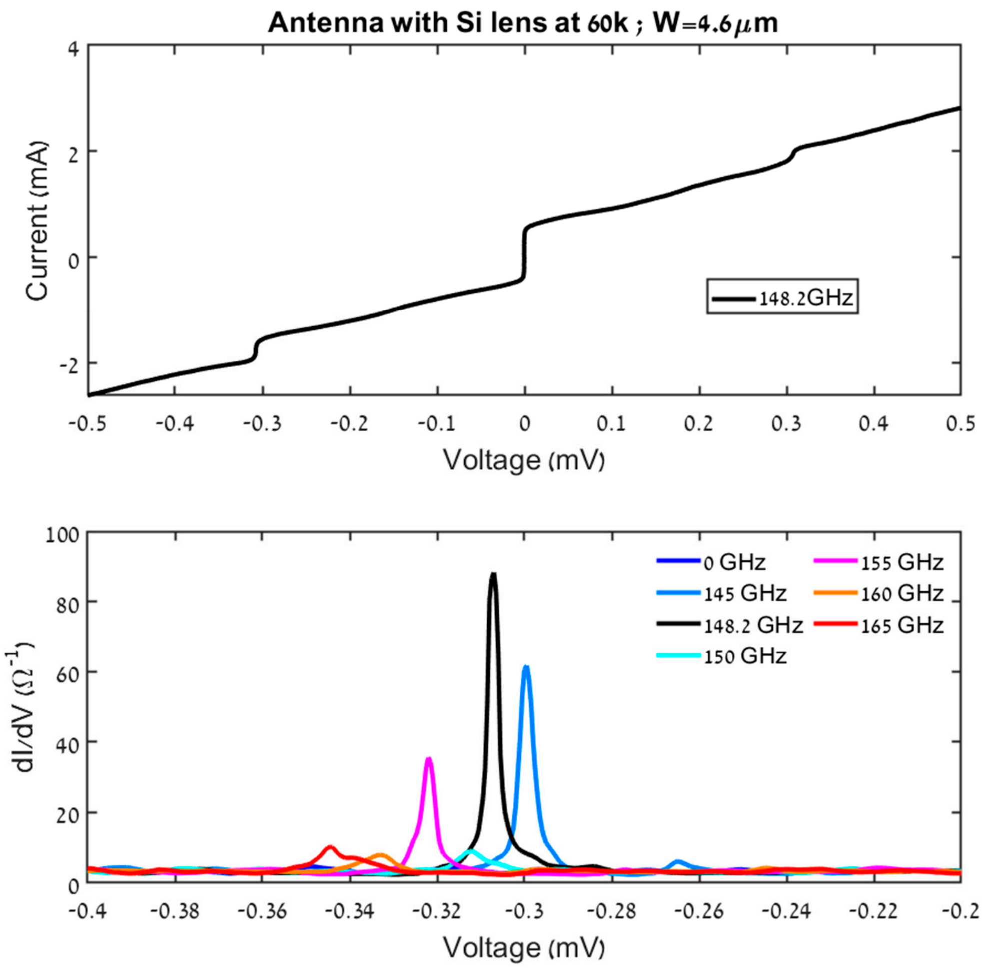

Figure 15. I-V (**top figure**) and dI/dV (**bottom figure**) characteristics measured at 60 K for an antenna with a 4.6 µm wide matching strip, with a Si lens.

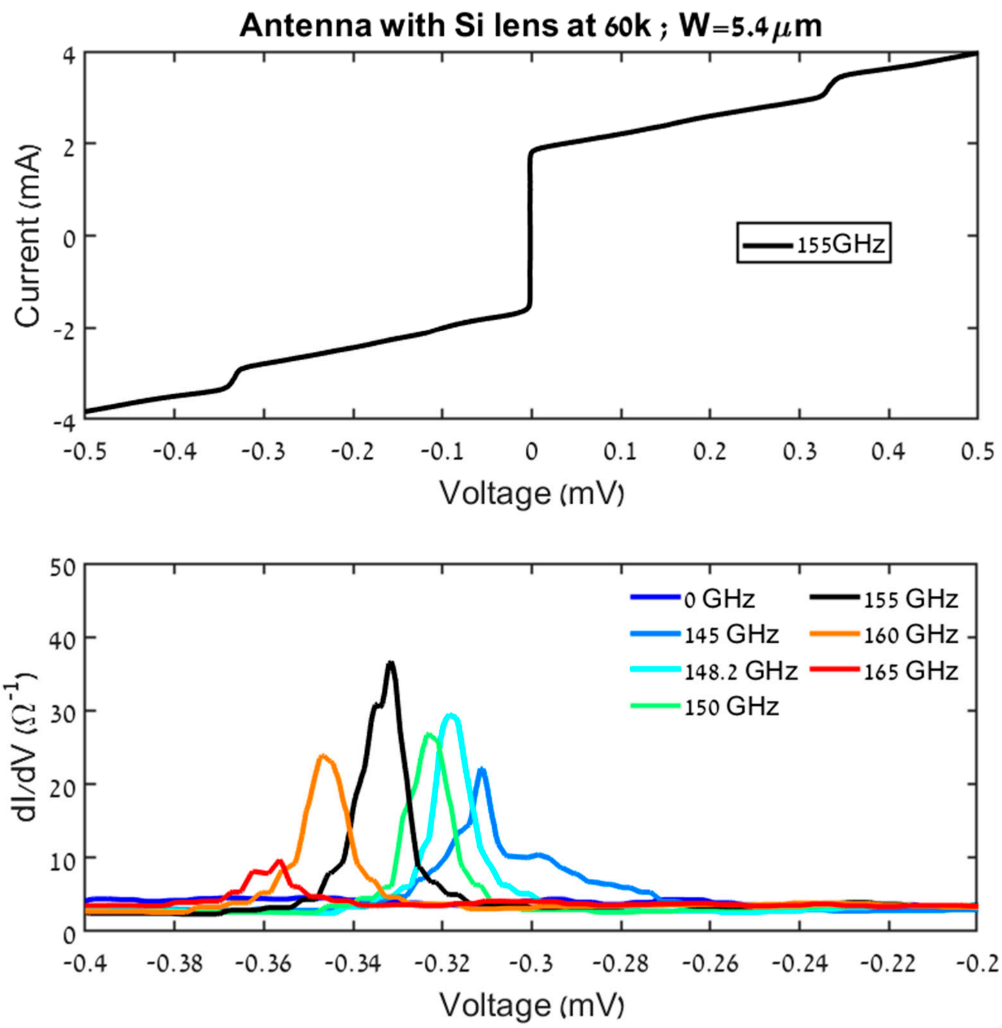

Figure 16. I-V (**top figure**) and dI/dV (**bottom figure**) characteristics measured at 60 K for an antenna with a 5.4 µm wide matching strips, with a Si lens.

4. Discussion

Several research groups report on sub-THz detection system based on YBCO Josephson junction detectors in a planar antenna configuration. Du et al. integrated a ring-slot [12,34,43] and log-periodic [44] planar antennas with relatively low input impedance (~30 Ω) for HTSC YBCO step-edge Josephson junctions, achieving a voltage responsivity $\eta(V) \approx 3.5$ kV·W^{-1} and an estimated NEP of ~1×10^{-12} W·Hz$^{-1/2}$ at 60 K. Additional structures were presented by Nakajima et al. [45] and Gao et al. [46,47]. They were able to obtain planar antennas with low input impedance (~13 Ω) combined with YBCO grain-boundary Josephson Junctions detectors, using coplanar waveguide feeding. In our previous report, we investigated a rounded bow tie antenna based on a bicrystal Josephson junction detector [25], with neither a Si lens nor an impedance matching unit. With that system, we obtained a voltage responsivity of $\eta(V) \approx 1$ kV·W^{-1} and an estimated NEP of ~6×10^{-12} W·Hz$^{-1/2}$ at 60 K. In addition, we reported on a step-edge junction detector with a Si lens, without a matching unit, obtaining a voltage responsivity of $\eta(V) \approx 15$ kV·W^{-1} [18]. In comparison with previous results, the performance obtained with impedance matching technique presented in this study are significantly superior, showing an estimated NEP of ~1×10^{-13} W·Hz$^{-1/2}$ and voltage responsivity of $\eta(V) \approx 55$ kV·W^{-1}.

5. Conclusions

The performance of high frequency communication antennas for the sub-THz frequency range deteriorates rapidly by impedance mismatch. We designed a new structure in which a superior impedance matching can be obtained by placing the Josephson junction detector remote from the antenna center. Simulations in the range of 130 to 170 GHz for optimal configuration parameters demonstrate a high radiation gain and a low reflection coefficient, S_{11}.

Based on these simulations, we fabricated two bow-tie antennas with different matching strips widths: 4.6 µm and 5.4 µm. The measured performances of these antennas at 60 K, with and without a silicon lens, were analyzed. The experimental results agree extremely well with the simulation results. The high peaks in the various dI/dV characteristics, as well as the measured values of the NEP and $\eta(V)$, are a clear indication of the high sensitivity and frequency selectivity of the proposed detection systems. We have shown that this structure has the potential of improving significantly the detection system efficiency at the THz range.

The massive increase in use of communication networks, such as in the Fifth Generation (5G) technologies, leads to an ever-increasing demand for higher frequency communication ranges. New technologies must be implemented to enable handling the required communication capacity. Solving the problem of impedance mismatch between the HTSC detectors and the antenna presented in this work, is a significant step in the right direction.

Author Contributions: Conceptualization, E.H.; methodology, E.H.; electromagnetic simulations were performed by, E.H., M.M. and D.V.; resources, E.H., S.E.S. and E.F.; writing—original draft preparation, E.H.; writing—review and editing, S.E.S. and E.F.; experiments were performed by, E.H., A.G.M. and E.F.; data analysis, E.H. and A.G.M.; funding acquisition, S.E.S. and E.F. All authors have read and agreed to the published version of the manuscript.

Funding: This research received no external funding.

Conflicts of Interest: The authors declare no conflict of interest.

Appendix A

Figure A1 is a photo image of the measurement setup described in Section 3. The setup includes the BWO THz source (1), the quasi-optical lenses (2), the cryogenic cooling system with the polyethylene windows (3), and the Keithley Nano-voltmeter and current source (4). For data acquisition and analysis, the measurement equipment was connected to a computer unit. Additionally seen on the optical bench are a chopper and power attenuators (5) (not used in the present experiments). The picture was taken in the applied superconductivity and optical spectroscopy lab in Ariel University, Israel.

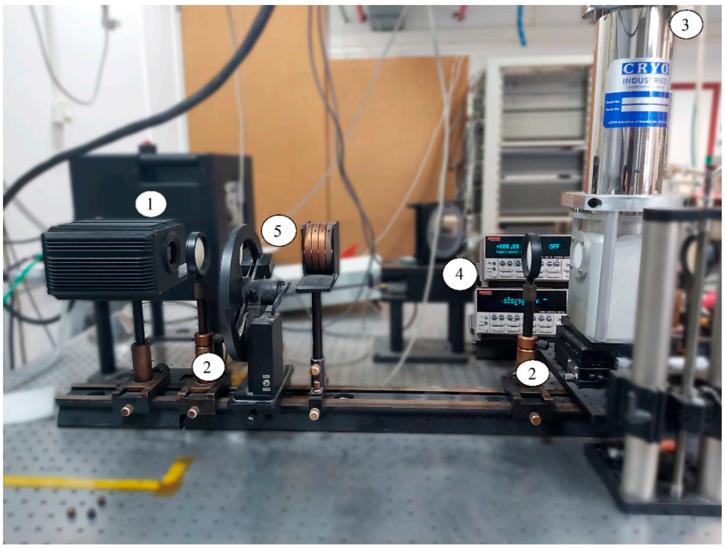

Figure A1. A photo image of the measurement setup.

References

1. Bogale, T.E.; Wang, X.; Le, L.B. mmWave communication enabling techniques for 5G wireless systems: A link level perspective. In *mmWave Massive MIMO: A Paradigm for 5G*, 1st ed.; Mumtaz, S.A.J., Rodriguez, B.L., Dai, C., Eds.; Elsevier Inc.: Houston, TX, USA, 2017; pp. 195–225.
2. Rogalski, A.; Sizov, F. Terahertz detectors and focal plane arrays. *Opto-Electron. Rev.* **2011**, *19*, 346–404. [CrossRef]
3. Delfanazari, K.; Klemm, R.A.; Joyce, H.J.; Ritchie, D.A.; Kadowaki, K. Integrated, portable, tunable, and coherent terahertz sources and sensitive detectors based on layered superconductors. *Proc. IEEE* **2020**, *108*, 721–734. [CrossRef]
4. Lewis, R.A. Review of terahertz detectors. *J. Phys. D Appl. Phys.* **2019**, *52*, 433001. [CrossRef]
5. Zhuang, L.; Rui, C.; Xiaohui, T.; Lihui, J.; Dawei, R. Terahertz sources, detectors, and transceivers in silicon technologies. In *Electromagnetic Materials and Devices*, 1st ed.; Man-Gui Han, A., Ed.; IntechOpen: London, UK, 2019; p. 86468.
6. Foley, C.P.; Mitchell, E.E.; Lam, S.K.H.; Sankrithyan, B.; Wilson, Y.M.; Tilbrook, D.L.; Morris, S.J. Fabrication and characterization of YBCO single boundary step edge junctions. *IEEE Trans. Appl. Supercon.* **1999**, *9*, 4281–4284. [CrossRef]
7. Richards, P.L. The Josephson junction as a detector of microwave and far infrared radiation. In *Semiconductors and Semimetals*; Academic Press: Cambridge, MA, USA, 1977; Volume 12, pp. 395–440.
8. Barone, A.; Paterno, G. *Physics and Applications of the Josephson Effect*, 1st ed.; Chapter 6, Chapter 11; John Wiley and Sons Inc.: Hoboken, NJ, USA, 1982; pp. 121–128, 309–310.
9. Van Duzer, T.; Turner, C.W. *Principles of Superconductive Devices and Circuits*, 2nd ed.; Chapter 4, Chapter 5; Prentice Hall PTR: Upper Saddle River, NJ, USA, 1999; pp. 206–209, 221–223.
10. Muyari, J.; Kobayashi, N.; Takahashi, S.; Hayashi, K.; Saito, A.; Ohshima, S. Fabrication process of YBCO thin film starting from amorphous film for microstrip line device. *Phys. Procedia* **2012**, *27*, 280–283. [CrossRef]
11. Holdengreber, E.; Mizrahi, M.; Glassner, E.; Dahan, Y.; Castro, H.; Farber, E. Design and implementation of an RF coupler based on YBCO superconducting films. *IEEE Trans. Appl. Supercond.* **2015**, *25*, 3–7. [CrossRef]
12. Du, J.; Hellicar, A.D.; Li, L.; Hanham, S.M.; Macfarlane, J.C.; Leslie, K.E.; Nikolic, N.; Foley, C.P.; Greene, K.J. Terahertz imaging at 77 K. *Supercond. Sci. Technol.* **2009**, *22*, 114001. [CrossRef]
13. Vasilić, B.; Shitov, S.V.; Lobb, C.J.; Barbara, P. Josephson-junction arrays as high-efficiency sources of coherent millimeter-wave radiation. *Appl. Phys. Lett.* **2001**, *78*, 1137–1139. [CrossRef]
14. Ivanchenko, Y.M. High-efficiency frequency generation in a periodic array of Josephson junctions. *Phys. Rev. B* **1996**, *54*, 13247–13260. [CrossRef]
15. Balanis, C.A. *Antenna Theory*, 3rd ed.; Chapter 9; John & Wiley & Sons: Hoboken, NJ, USA, 2005; pp. 500–504.
16. Lee, K.; Iguchi, I.; Constantinian, K.Y. Tunable detection of radiation from HTSC Josephson junction arrays. *Physica C* **1999**, *320*, 65–70. [CrossRef]
17. Kermorvant, J.; van der Beek, C.J.; Mage, J.C.; Marcilhac, B.; Lemaître, Y.; Briatico, J.; Bernard, R.; Villegas, J. Joule heating and high frequency nonlinear effects in the surface impedance of high Tc superconductors. *J. Appl. Phys.* **2009**, *106*, 023912. [CrossRef]
18. Holdengreber, E.; Gao, X.; Mizrahi, M.; Schacham, S.E.; Farber, E. Superior impedance matching of THz antennas with HTSC josephson junctions. *Supercond. Sci. Technol.* **2019**, *32*, 074006. [CrossRef]
19. Bozovic, I.; Logvenov, G.; Verhoeven, M.A.J.; Caputo, P.; Goldobin, E.; Beasley, M.R. Giant proximity effect in cuprate superconductors. *Phys. Rev. Lett.* **2004**, *93*, 157002. [CrossRef] [PubMed]
20. Compton, R.C.; McPhedran, R.; Popovic, Z.; Rebeiz, G.; Tong, P.; Rutledge, D. Bow-tie antennas on a dielectric half-space: Theory and experiment. *IEEE Trans. Antennas Propag.* **1987**, *35*, 622–631. [CrossRef]
21. Batov, I.E.; Jin, X.Y.; Shitov, S.V.; Koval, Y.; Müller, P.; Ustinov, A.V. Detection of 0.5THz radiation from intrinsic Bi2Sr2CaCu2O8 Josephson junctions. *Appl. Phys. Lett.* **2006**, *88*, 262504. [CrossRef]
22. Kaur, B.; Solanki, L.S. A brief review on bow-tie antenna. In Proceedings of the NCCN 12th Annual Congress: Hematologic Malignancies, San Francisco, CA, USA, 6–7 October 2017; pp. 3–4.
23. Alharbi, K.; Ofiare, H.A.; Kgwadi, M.; Khalid, A.; Wasige, E. Bow-tie antenna for terahertz resonant tunnelling diode based oscillators on high dielectric constant substrate. In Proceedings of the 2015 11th Conference on Ph.D. Research in Microelectronics and Electronics (PRIME), Glasgow, Scotland, 29 June–2 July 2015; pp. 168–171.

24. Aji, A.P.; Apriono, C.; Zulkifli, F.Y.; Rahardjo, E.T. Radiation pattern validation of a THz planar bow-tie antenna at microwave domain by scaling up technique. In Proceedings of the 2017 International Conference on Radar, Antenna, Microwave, Electronics, and Telecommunications (ICRAMET), Jakarta, Indonesia, 23–24 October 2017; pp. 108–111.
25. Holdengreber, E.; Moshe, A.G.; Mizrahi, M.; Khavkin, V.; Schacham, S.E.; Farber, E. High sensitivity high Tc superconducting Josephson junction antenna for 200 GHz detection. *J. Electromagnet. Wave.* **2019**, *33*, 193–203. [CrossRef]
26. Yu, M.; Chen, Z.N.; Xu, W.W.; Xu, Y.C.; Geng, H.F.; Hua, T.; Wu, P.H. Impedance matching of bow-tie antenna for high temperature superconducting YBCO Josephson junction mixer. In Proceedings of the 2017 42nd International Conference on Infrared, Millimeter, and Terahertz Waves (IRMMW-THz), Cancun, Mexico, 27 August–1 September 2017; pp. 1–2.
27. Holdengreber, E.; Mizrahi, M.; Khavkin, V.; Schacham, S.E.; Farber, E. Improved THz reception by non-conventional structure of planar dipole antenna with superconducting Josephson junction detector. In Proceedings of the IEEE International Conference on Microwaves, Antennas, Communications and Electronic Systems (COMCAS), Tel-Aviv, Israel, 4–6 November 2019; pp. 1–4.
28. Holdengreber, E.; Mizrahi, M.; Schacham, S.E.; Farber, E. Remote location of superconducting Josephson junction in planar antennas for improved THz detection. In Proceedings of the 2019 IEEE International Superconductive Electronics Conference (ISEC), Riverside, CA, USA, 28 July–1 August 2019; pp. 1–5.
29. Holdengreber, E.; Schacham, S.E.; Farber, E. Impedance mismatch elimination for improved THz detection by superconducting Josephson junctions. In Proceedings of the Antennas and Propagation Conference 2019 (APC-2019), Birmingham, UK, 11–12 November 2019; pp. 1–3.
30. Yu, M.; Geng, H.; Hua, T.; Xu, W.; Chen, Z.N. Reactance matching for superconducting YBCO Josephson junction detector using bowtie antenna. In Proceedings of the 2018 IEEE Asia-Pacific Conference on Antennas and Propagation (APCAP), Auckland, New Zealand, 5–8 August 2018; pp. 1–2.
31. Winkler, D.; Zhang, Y.M.; Nilsson, P.A.; Stepantsov, E.A.; Claeson, T. Electromagnetic properties at the grain boundary interface of a YBa2Cu307 bicrystal Josephson junction. *Phys. Rev. Lett.* **1994**, *72*, 1260–1263. [CrossRef]
32. Theva GmbH, Germany. Available online: www.theva.com (accessed on 5 November 2019).
33. STAR Cryoelectronics, USA. Available online: www.starcryo.com (accessed on 22 February 2020).
34. Du, J.; Hellicar, A.D.; Li, L.; Hanham, S.M.; Nikolic, N.; Macfarlane, J.C.; Leslie, K.E. Terahertz imaging using a high-T_C superconducting Josephson junction detector. *Supercond. Sci. Technol.* **2008**, *21*, 125025. [CrossRef]
35. Taur, Y.; Richards, P.L.; Auracher, F. Application of the shunted junction model to point-contact Josephson junctions. *Low Temp. Phys.* **1974**, *3*, 276–281.
36. Han, J.; Woo, B.K.; Chen, W.; Sang, M.; Lu, X.; Zhang, W. Terahertz dielectric properties of MgO nanocrystals. *J. Phys. Chem. C* **2008**, *112*, 17512–17516. [CrossRef]
37. Phillips, J.M. Substrate selection for high-temperature superconducting thin films. *J. Appl. Phys.* **1996**, *79*, 1829–1848. [CrossRef]
38. Beck, A.; Stenzel, A.; Froehlich, O.M.; Gerber, R.; Gerdemann, R.; Alff, L.; Mayer, B.; Gross, R. Fabrication and superconducting transport properties of bicrystal grain boundary Josephson junctions on different substrates. *IEEE Trans. Appl. Supercond.* **1995**, *5*, 2192–2195. [CrossRef]
39. Hailu, D.M.; Ehtezazi, I.A.; Neshat, M.; Safavi-Naeini, S. Simulation of bow-tie THz antenna using hybrid finite element method and spectral ray tracing technique. In Proceedings of the 34th International Conference on Infrared, Millimeter, and Terahertz Waves, Busan, Korea, 21–25 September 2009.
40. Rutledge, D.; Muha, M. Imaging antenna arrays. *IEEE Trans. Antennas Propag.* **1982**, *30*, 535–540. [CrossRef]
41. Kozlov, G.; Volkov, A. Millimeter and submillimeter wave spectroscopy of solids, Coherent source submillimeter wave spectroscopy. In *Topics in Applied Physics*, 1st ed.; Grüner, G., Ed.; Springer: New York, NY, USA, 1998; pp. 52–109.
42. Hesler, J.L.; Crowe, T.W. NEP and responsivity of THz zero-bias Schottky diode detectors. In Proceedings of the 2007 Joint 32nd International Conference on Infrared and Millimeter Waves and the 15th International Conference on Terahertz Electronics, Cardiff, UK, 2–9 September 2007; pp. 844–845.
43. Du, J.; Smart, K.; Li, L.; Leslie, K.E.; Hanham, S.M.; Wang, D.H.C.; Foley, C.P.; Ji, F.; Li, X.D.; Zeng, D.Z. A cryogen-free HTS Josephson junction detector for terahertz imaging. *Supercond. Sci. Technol.* **2015**, *28*, 084001. [CrossRef]

44. Du, J.; Hellicar, A.D.; Hanham, S.M.; Li, L.; Macfarlane, J.C.; Leslie, K.E.; Foley, C.P. Terahertz and millimetre wave imaging with a broadband Josephson detector working above 77 K. *J. Infrared. Milli. Terahz. Waves* **2011**, *32*, 681–690. [CrossRef]
45. Nakajima, K.; Ebisawa, N.; Sato, H.; Chen, J.; Yamashita, T.; Sawaya, Y. Millimeter-wave sensitivity of YBCO grain boundary Josephson junctions coupled with coplanar waveguide-fed slot dipole antennas. *IEEE Trans. Appl. Supercond.* **2005**, *15*, 549–551. [CrossRef]
46. Gao, X.; Zhang, T.; Du, J.; Guo, Y.J. 340 GHz double-sideband mixer based on antenna-coupled high-temperature superconducting Josephson junction. *IEEE Trans Terahertz Sci Technol.* **2020**, *10*, 21–31. [CrossRef]
47. Gao, X.; Du, J.; Zhang, T.; Guo, Y.J. High-Tc superconducting fourth-harmonic mixer using a dual-band terahertz on-chip antenna of high coupling efficiency. *IEEE Trans. Terahertz Sci. Technol.* **2019**, *9*, 55–62. [CrossRef]